Article

Volume 14, Issue 3, 2025, 107

https://doi.org/10.33263/LIANBS143.107

Applications of Silver Nanoparticles Photosynthesized from the Agricultural Waste *Durio Zibethinus* Peels

Trung Dien Nguyen ^{1,*} An Ngoc Phan ¹, Hong Thi Nguyen ², Nhung Thi-Tuyet Thai ¹, Gia Thi-Ngoc Trinh ¹

- ¹ School of Education, Can Tho University, 3/2 Street, Ninh Kieu, Can Tho City, 94000, Vietnam
- College of Natural Sciences, Can Tho University, 3/2 Street, Ninh Kieu, Can Tho City, 94000, Vietnam
- * Correspondence: ndtrung@ctu.edu.vn;

Received: 20.08.2024; Accepted: 11.04.2025; Published: 4.09.2025

Abstract: The objective of the ongoing study is to present plant extract and irradiation dual-assisted synthesis of silver nanoparticles. *Durio zibethinus* peel extract functioned effectively both as a reducing agent and stabilizer under light-emitting diode-artificial sunlight. Several tests were conducted to explore the optimal parameters, including the concentration of *Durio zibethinus* peel extract, the temperature used for extraction, and the duration of extraction, which were closely related to the formation and stability of the plant extract-synthesized nanosilver. The green-synthesized material was pure silver phases and dispersed uniformly in spherical shapes with an average size of 17.4 nm. Antimicrobial activities of negatively spherical nanoparticles (–25.6 mV) were briefly covered in the negative-gram bacteria (*Escherichia coli, Pseudomonas aeruginosa*, and *Salmonella enterica*), positive-gram bacteria (*Bacillus subtilis, Lactobacillus fermentum*, and *Staphylococcus aureus*), and cancer cells (Human oral KB, Hepatoblastoma-derived HepG2, Lung A549, and Breast MCF7). The extract-assisted silver nanoparticles exhibited a highly significant inhibition against *Pseudomonas aeruginosa*, *Lactobacillus fermentum*, and MCF7. Additionally, the produced silver nanoparticles were also utilized to determine Cu²⁺ by colorimetric method with a limit of detection at 1.8 μg/L.

Keywords: antimicrobial activity; colorimetric detection; *Durio zibethinus* peels; light-emitting diodeartificial sunlight; silver nanoparticles.

© 2025 by the authors. This article is an open-access article distributed under the terms and conditions of the Creative Commons Attribution (CC BY) license (https://creativecommons.org/licenses/by/4.0/), which permits unrestricted use, distribution, and reproduction in any medium, provided the original work is properly cited. The authors retain copyright of their work, and no permission is required from the authors or the publisher to reuse or distribute this article, as long as proper attribution is given to the original source.

1. Introduction

In the present age, the emergence of nanotechnology has drawn numerous scientists' attention due to its characteristic properties and a series of applications in multitudinous fields of chemistry [1], medicine [2], microbiology [3], technology [4], and the environment [5]. Gold, silver, and copper have become the most desirable metallic nanoparticles owing to their exclusive properties. Silver compounds have strong oxidation abilities to treat varied bacterial infections [6]. However, since many antibiotics had first come on the market, the use of these silver compounds drastically decreased. Scientists tried reducing metals to their nanoscale, significantly altering their chemical, physical, and optical natures. Silver nanoparticles (AgNPs), whose diameters range from 1 to 100 nanometers, have become promising antimicrobial agents [7]. AgNPs possess the capability to invade the bacterial cell wall, alter the structure of cell membranes, and even cause cell death. As a result, the techniques for

creating AgNPs emerged with a range of biomedicinal applications, including antibacterial [7], antifungal [8], and anticancer activity [9].

The properties and stability of synthesized AgNPs depend on various factors, such as shape, size, and surface charge [10]. AgNPs are more fragile, prone to oxidation, and capable of forming massive clusters. Hence, exploring synthetic methods that allow for control of the shape, size, and surface charge of produced AgNPs has recently received much attention. Several techniques have been developed involving physical, chemical, and green synthesis for AgNP formation [11]. Both "Top-down" and "Bottom-up" methodologies are used to create AgNPs [12]. In the "Top-down" procedure, suitable bulk silver is broken into small particles by size reduction using physical processes, while the "Bottom-up" procedure involves the application of multiple chemical and biological treatments through the self-assembly of atoms to newly generated nuclei, which eventually form into nanoscale particles [13]. Regardless of the techniques followed, the general principle is to convert silver ions Ag⁺ dissolved in silver salt solutions into silver atoms Ag⁰, through chemical reduction. With chemical methods, sodium citrate (Na₃C₆H₅O₇), sodium borohydride (NaBH₄), and hydrazine (N₂H₄) were known as the most powerful chemical reducing agents employed in the synthesis of AgNPs [14]. Nonetheless, these agents are expensive and have environmental toxicity [11]. Similarly, physical methods involve expensive types of equipment and waste a lot of energy when using physical agents that employ high-energy electromagnetism and electromagnetic waves, such as gamma radiation [15], UV radiation [16], and laser radiation [17]. In addition, it is also a time-consuming process to raise the ambient temperature surrounding the source material to achieve thermal stability [18]. Consequently, green synthesis routes utilizing plant extracts are considered to have tremendously outstanding advantages due to their eco-friendly, straightforward, and non-toxic manufacturing procedure. In particular, phytoconstituents extracted from bio-organisms not only play an essential role as a reducing agent but also act as a capping agent that could attach to the surface of AgNPs [19].

Durian (Durio zibethinus Murr., Family: Bombacaceae, Genus: Durio) is the prominent tropical fruit of Southeast Asian countries and is known as the "King of Fruit" because of its exclusive odor and offensive taste. Vietnam's Durio zibethinus (D. zibethinus) output has recently expanded dramatically, becoming an important source of revenue for farmers who reside in fruit-growing regions [20]. An average D. zibethinus' mass ranges from 1 to 3 kg. However, the weight of the residue only makes up 60-70% of the total weight of the fruit, which leads to a massive amount of agricultural waste [21]. In an attempt to solve this problem, researchers have conducted several studies about making use of D. zibethinus peels for their translation into valuable nanomaterials [22]. The existence of flavonoids, polysaccharides, phenolic acids, phenolic glycosides, and pectin in the extract's chemical constituents plays an important role in the formation and stabilization of AgNPs [23]. Meanwhile, pectin, which was found in various fruit remnants, has been recently investigated for its potential in the formation of metal nanoparticles. The hydroxyl and methoxyl groups within the structure of pectin functioned as reductants in the biosynthesis and stabilization of AgNPs [24]. Recently, D. zibethinus peel extract has been considered for use in synthesizing AgNPs. Alzahrani's research synthesized AgNPs from durian shell aqueous solution to detect the presence of ammonia at low concentrations [22]. The outcomes showed that fabricated AgNPs had an average size of around 25 nm and detected ammonia at 500 ppm concentrations. Another study, producing AgNPs from the durian ring extract with fluorescent light bulb assistance, was published by

Chutrakulwong [25]. TEM images showed that the produced AgNPs were spherical with a small particle size of about 10 nm and possessed extraordinary stability.

Besides, the photoreduction of silver salts also benefits from the support of light sources, including fluorescent light, LED, laser, and sunlight [26-29]. Numerous advantages have emerged for these light-driven processes, including improved optical properties, well-controlled morphology, excellent photon efficacy, and energy stability [27]. Plenty of research on photoinduced techniques has been conducted. Chutrakulwong was successful in obtaining spherical AgNPs for 5 min utilizing biomass made from durian rind exposed to sunlight [25]. Likewise, Lee productively studied AgNP synthesis employing *Dryopteris crassirhizoma rhizome* extract under various sources of light [27]. The altered color of the plant extract after 30-minute irradiation was attributed to the presence of AgNPs. Compared with other lights, LED artificial sunlight makes it easier to control the intensity and is more affordable due to its low energy consumption [30].

This work is the first to study a green-synthesized approach using D. zibethinus peel extract assisted under LED artificial sunlight. Synthesis conditions for AgNP formation, including the influence of the concentration of D. zibethinus peel extract, the temperature used for extraction, and the duration of extraction, were estimated. Additionally, there is a comprehensive investigation into the efficient synthesis and stability of the produced AgNPs. Finally, the characteristics of the green-synthesized AgNPs, such as antimicrobial activities and colorimetric assays for Cu^{2+} detection, were considered in detail.

2. Materials and Methods

2.1. Materials.

Fresh and ripe *D. zibethinus* peels were procured at a local market (Can Tho, Vietnam). Merck-procured silver nitrate AgNO₃ was employed as the precursor for synthesizing AgNPs. Throughout the investigation, double-distilled water was used as a solvent to prepare the solutions and extract them. Copper nitrate Cu(NO₃)₂ with a concentration of 1000 mg/L prepared in nitric acid HNO₃ 0.5 M from Merck was used as the copper standard.

2.2. Preparing D. zibethinus peel extract.

The fresh and ripe *D. zibethinus* peels were rinsed under distilled water to purify the surface. The following stage was the removal of the exocarp (green parts), accumulating the mesocarp and the endocarp (white parts), and cutting them into small pieces. The collected residues were dried at 80°C for 48 h, milled into fine powders using a mechanical grinder, and preserved at 4°C for additional use. An adequate amount of prepared *D. zibethinus* peel powder was boiled with 100 mL of double-distilled water at the determined temperature and required duration for extraction to become a heterogeneous mixture. The extract was purified through Whatman paper and subjected to centrifugation at 6800 rpm for 60 min to eliminate solid residue. It was then used for nanomaterial synthesis.

2.3. Synthesizing AgNPs.

AgNP formation was integrated by dissolving a constant amount of silver nitrate at 1 mM in the *D. zibethinus* peel extract with LED photoirradiation for 2 h. Nanomaterial was formed by the presence of LED light, denoted as AgNPsDz-SLL. The color of the homogenous

solution, converted from pale yellow to yellow-brown, determined the existence of AgNPs. The concentration of silver nitrate was kept at 1 mM in all experiments, whereas the effects of the alternated concentration of *D. zibethinus* peel powder (1, 3, 5, 7, and 9 g/L), temperature used for extraction (30, 40, 50, 60, and 70°C), and duration of extraction (5, 10, 20, 30, and 45 min) on the AgNPsDz-SLL synthesis were investigated to specify the finest condition for the procedure.

2.4. Characterization of the produced AgNPs.

The ultraviolet-visible (UV-Vis) spectrophotometer (V-730, Jasco) was used to recognize the presence of AgNPs and evaluate the durability of AgNPsDz-SLL. The morphology and size of the produced AgNPs were characterized by a JEOL-1400 transmission electron microscope (TEM). Further, the crystal structure of AgNPs was verified using a Bruker D2 Phaser X-ray diffractometer (XRD) instrument operated at a voltage of 40 kV and a current of 40 mV using CuK_{α} radiation. A particle electrophoresis apparatus (Zetasizer instrument, Malvern, Nano ZS) was utilized to evaluate the stability and measure the surface charge of AgNPs. The presence of functional groups in the *D. zibethinus* peel extract and synthesized AgNPs was determined by Fourier-transform infrared (FTIR) spectroscopy. An inductively coupled plasma optical emission (ICP-OES) spectroscopy was used to determine the presence of Ag⁺ in the precursor and AgNPsDz-SLL to evaluate the efficiency of synthesis. The reaction efficiency (H) under the optimal condition was determined using the following formula (1).

$$H = \frac{C_o - C_r}{C_o} \times 100 \tag{1}$$

Where C_o and C_r are the Ag^+ ion initial concentrations and Ag^+ ion residual concentrations, respectively.

2.5. Antibacterial activity of the photosynthesized AgNPs.

The antimicrobial activity of the synthesized AgNPsDz-SLL was evaluated against gram-negative bacteria, including *Escherichia coli* (*E. coli* ATCC 25922), *Pseudomonas aeruginosa* (*P. aeruginosa* ATCC 15442), and *Salmonella enterica* (*S. enterica* ATCC 35664), as well as gram-positive bacteria, including *Bacillus subtilis* (*B. subtilis* ATCC 6633), *Lactobacillus fermentum* (*L. fermentum* N4), and *Staphylococcus aureus* (*S. aureus* ATCC 13709). Trypticase soy broth and trypticase soy agar were used in the quantitative growth experiments of bacteria. Following the 0.5 McFarland standard, bacteria strains with 5×10⁵ CFU/mL were subcultured onto agar plates at 37°C-24 h. Ampicillin and cefotaxime were employed in the standard antibiotic disks to suppress positive-gram and negative-gram microorganisms, respectively. After incubation, the plates were assessed for inhibition zone via the 50% inhibition concentration (IC₅₀) at 630 nm absorbance.

2.6. Anticancer activity of the plant-mediated AgNPs.

Various cancer cells, including Lung (A549), Hepatoblastoma-derived (HepG2), Human oral (KB), and Breast (MCF7), were consistently studied with different concentrations to assess the anticancer efficacy of AgNPsDz-SLL. Cancer cell lines were subcultured in Dulbecco's modified Eagle's medium (DMEM) with 10% fetal bovine serum (FBS) and 1%

penicillin-streptomycin. The cultured cells were kept in a humidified incubator with 5% CO₂ at 37°C. Trypan blue was used to stain the cells, and the number of viable cells was counted using a hemocytometer. The cancer cells were cultivated in a 96-well plate at a density of 3×10⁴ CFU/well for 72 h. A549, HepG2, KB, and MCF7 cancer cells were examined with altered concentrations: 1, 4, 16, and 64 mg/L for biosynthesized AgNPs. The solvent used in the control culture was dimethyl sulfoxide. The cancer cell lines were cultivated and incubated at 37°C-72 h in a humidified incubator with 5% CO₂. Thereafter, 100 mg/mL MTT reagent was aspirated, and the formazan crystals were dissolved by adding 100 μL of dimethyl sulfoxide. The homogeneous solution was further incubated at 37°C-4 h. In this study, all control samples contained an equal amount of Ellipticine, and the optical density of the studied samples was determined using a 96-well plate reader microplate at a wavelength of 540 nm. The activity of cancer cell viability inhibition was computed using the following equation (2) [31].

$$I = \frac{A_{\text{sample}} - A_{\text{blank}}}{A_{\text{control}} - A_{\text{blank}}} \times 100$$
 (2)

where I is the percentage of inhibition. The absorbances of the tested, blank, and control samples are denoted by A_{sample} , A_{blank} , and $A_{control}$, respectively.

2.7. Colorimetric detection of Cu^{2+} .

AgNPsDz-SLL were centrifuged at 6800 rpm-4 h to separate the extract, and the collected nanoparticles were completely dispersed into water. Standard solution $Cu(NO_3)_2$ was diluted in water to obtain a solution of Cu^{2+} of 10 mg/L. At first, to create a 3900 μ L Cu^{2+} solution with various concentrations, x μ L of 10 mg/L Cu^{2+} was mixed with water until the total volume reached 3900 μ L. Then, the desired concentration of Cu^{2+} was achieved by introducing 100 μ L of AgNPsDz-SLL to 3900 μ L of Cu^{2+} . Finally, the absorbance of the asprepared solutions was recorded in the wavelength range of 300-700 nm. The detection limit of Cu^{2+} , indicated as LOD, was calculated according to the formula (3).

$$LOD = \frac{3.3 \times SD}{h}$$
 (3)

where SD is the standard deviation of the curve and b is the slope of the calibration curve.

3. Results and Discussion

3.1. Synthesizing AgNPsDz-SLL.

Figure 1 presents the UV-Vis spectrum of 1 mM AgNO₃ (Ag), 3 g/L of *D. zibethinus* peel extracted at 60°C-30 min (DzExt), solution of 1 mM AgNO₃ and DzExt (Ag-DzExt), and solution of 1 mM AgNO₃ and DzExt with LED-artificial sunlight irradiation (Ag-DzExt-SLL). The surface plasmon resonance (SPR) appeared on Ag-DzExt and Ag-DzExt-SLL, while Ag and DzExt were absent from SPR. As can be seen, the presence of colloidal AgNPs on the prepared samples showed an SPR around 422 nm, characterizing AgNPs [32-34]. In addition, the peak intensity increased with the support of LED-sunlight irradiation, indicating that higher AgNPs were produced. From the initial investigation, LED-sunlight exhibited an effective enhancement in the rate of conversion of Ag⁺ into Ag⁰, followed by some research [25, 28]. Thus, LED artificial sunlight was considered for further utilization.

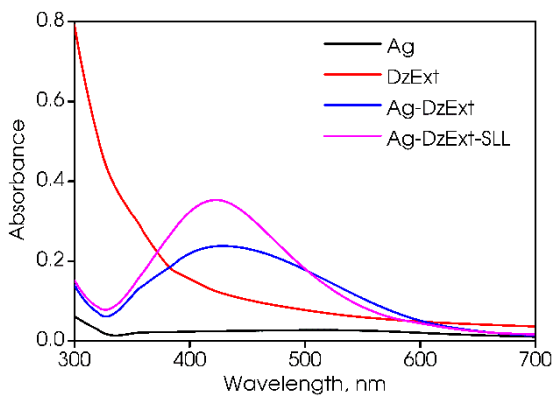


Figure 1. UV-Vis spectra of the initial investigation for photosynthesizing AgNPs.

The effects of *D. zibethinus* peel concentration, extraction temperature, and extraction time on the formation of AgNPs are shown in Figure 2. The effect of *D. zibethinus* peel concentration of 1-9 g/L prepared at 60°C-30 min on the AgNPs synthesis was scrutinized under LED-sunlight irradiation for 2 h. As Figure 2a illustrates, the measured absorption spectra at the above concentrations show that the SPR was blueshifted with a higher intensity with increasing concentration of *D. zibethinus* peel. The more reducing/stabilizing agents used, the more AgNPs formed [35]. The lowest and broadest SPR peak in the visible regions was observed at 1 g/L and increased considerably in a range of 3-9 g/L. The absorbance SPR peaks became sharper with the *D. zibethinus* peel powder above 5 g/L. Furthermore, the spectra of samples prepared at 5, 7, and 9 g/L with SPR peaked at around 423 nm, which demonstrated there was an insignificant shift in the particle size of AgNPs [36]. However, there was a slight enhancement in absorbance from 7 to 9 g/L (0.505 compared to 0.534). Therefore, the optimal concentration of *D. zibethinus* peel for the further experiment was chosen as 7 g/L.

Following the concentration of *D. zibethinus* peel, the extraction temperature was also a crucial parameter for testing. Figure 2b shows the effect of the temperature used for extraction (30-70°C) on AgNP fabrication. The extract of 7 g/L *D. zibethinus* peel was prepared at 60°C-30 min. Mixtures of the extract with AgNO₃ were subjected to LED sunlight exposure at room temperature for 2 h. It was recorded that the absorbance intensity increased significantly from 30 to 40°C. Nevertheless, there was a steady decrease in the value of the AgNPs absorbance at 60 and 70°C. More phenolic constituents in the extract were soluble at higher extraction temperatures, which was advantageous for forming metallic nanoparticles. Notwithstanding, there was competition for complexation with the presence of more phytochemicals in the extract, resulting in decreased AgNP formation [37]. Therefore, the optimal extraction temperature for the present work was 40°C.

The varied extraction time of *D. zibethinus* peel from 5 to 45 min was tested with other unchanged factors. Figure 2c shows a comparison of the SPR value of the synthesized samples. A significant rise in absorbance was recognized by extending the duration of extraction from 5 to 20 min. Having lengthened the duration of extraction, more phytocomponents were produced to enhance the conversion of Ag⁺ to Ag⁰. These results were compared with the research by Vishwasrao using sapota fruit waste for AgNP synthesis [38]. The absorbance of samples slightly increased from 0.564 to 0.594, corresponding to a variation in extraction time from 20 to 45 min. Thus, 20 min was selected as the appropriate extraction time.

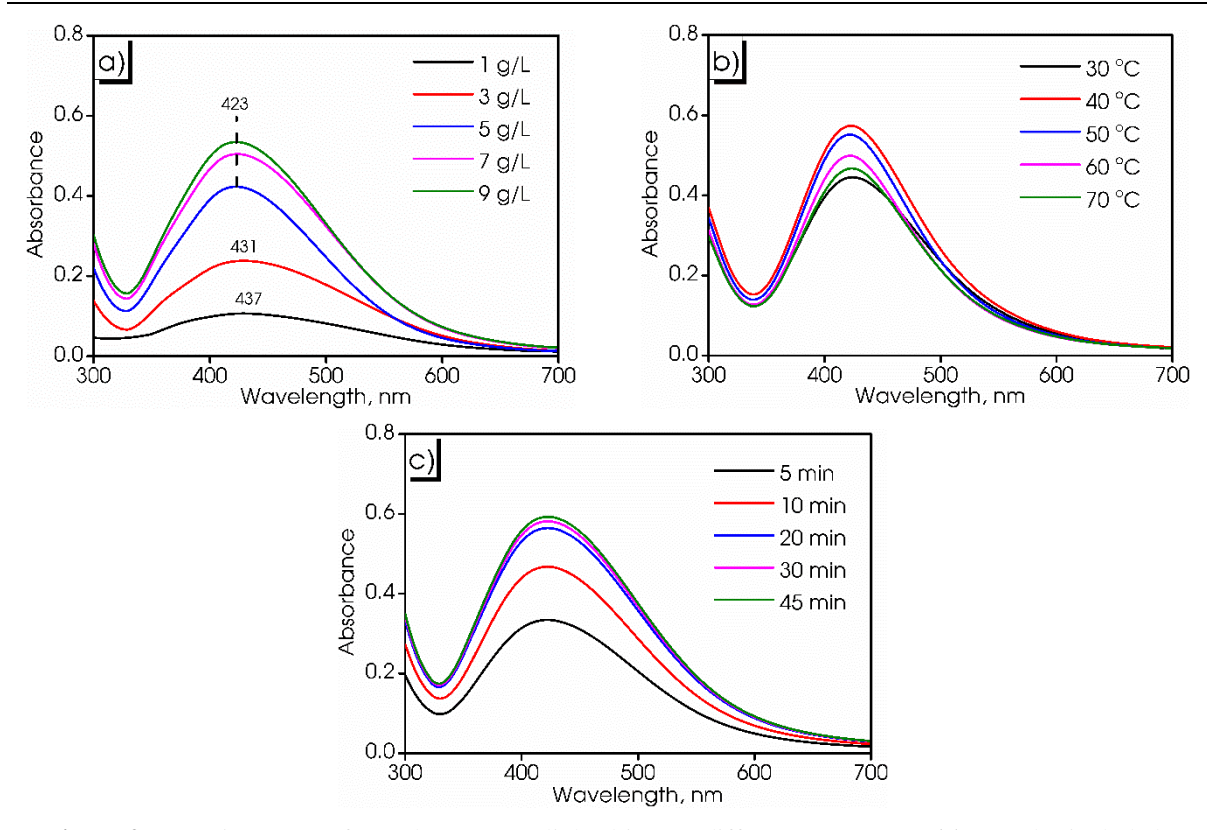


Figure 2. UV-Vis spectra of samples were sunlight-driven at different parameters: (a) Samples included 1 mM AgNO₃ with 1-9 g/L of *D. zibethinus* peel extracted at 60°C for 30 min irradiated by LED sunlight for 2 h; (b) Samples included 1 mM AgNO₃ with 7 g/L of *D. zibethinus* peel extracted at 30-60°C for 30 min irradiated by LED sunlight for 2 h; (c) Samples included 1 mM AgNO₃ with 7 g/L of *D. zibethinus* peel extracted at 40°C for 5-45 min irradiated by LED sunlight for 2 h.

The optimum conditions for the AgNPsDz-SLL synthesis were selected to be 7.0 g/L of D. zibethinus peel extracted at 40°C-20 min. Comparing the residual concentration of Ag⁺ ion in the synthesized AgNPsDz-SLL with the concentration of Ag⁺ ion in the precursor 1 mM AgNO₃ to determine reaction efficiency. The obtained results in Table 1 revealed that AgNPsDz-SLL reached a reaction efficiency of 83.4% with an AgNPs concentration of 72.4 mg/L.

Table 1. The concentration of Ag⁺ from the ICP-OES measurement.

Sample	Ag ⁺ concentration, mg/L	Reaction efficiency, %	AgNPs concentration, mg/L
AgNO ₃	86.8		
AgNPsDz-SLL	14.4	83.4	72.4

3.2. Characteristics of AgNPsDz-SLL.

The stability of the synthesized AgNPs-SLL was measured for ten weeks using the UV-Vis technique. As the storage time was extended for the duration of ten weeks, the characteristic SPR bands slightly fluctuated, which proved that nanoparticles could remain stable (Figure 3). Notably, a gradual rise in the absorbance was seen as storage time was prolonged, which specified that AgNPs were continuously produced. Due to an incomplete reaction, numerous reductants/stabilizers in the extract and residual Ag⁺ ions [39, 40].

Figure 4 illustrates the crystal structure of the synthesized AgNPsDz-SLL on the X-ray diffraction patterns. In the 2θ range from 20 to 80° , AgNPsDz-SLL possessed four diffraction peaks that were noted at 38.15° , 44.14° , 64.54° , and 77.53° . These peaks corresponded with

(111), (200), (220), and (311) planes of crystalline silver, which could be inferred from the face-centered cubic structure of silver metal (JCPDS No. 89-3722).

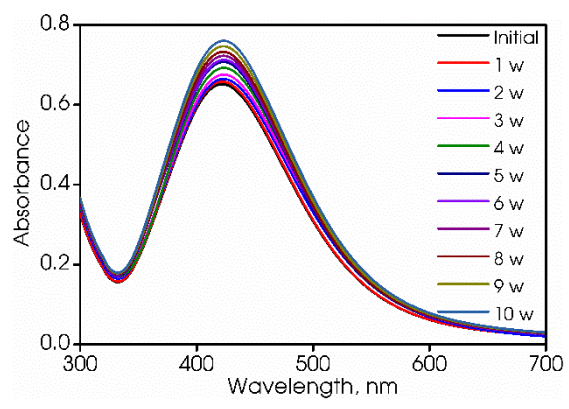


Figure 3. UV-Vis spectra of AgNPsDz-SLL according to the storage time.

The same findings were fabricated in Gopinath's research, in which AgNPs were synthesized utilizing *Pseudomonas putida* cell membranes derived from soil [41]. Moreover, the average crystallite size was calculated from the full width at half maximum (FWHM) of the diffraction peaks using the following Scherrer equation (4).

$$D = \frac{k \times \lambda}{\beta \times \cos \theta} \tag{4}$$

Where D is the average crystallite size, K means Scherrer's constant (K = 0.9), λ represents the CuK_{α} radiation's wavelength, β symbolizes FWHM in radians, and θ signifies the angle of the diffraction signal.

The width at half peak height was calculated from the Gaussian distribution associated with the peak values. The computed values for the phase composition and the crystallite size of AgNPsDz-SLL are listed in Table 2. The result revealed that the crystallite size of AgNPsDz-SLL was 14.6 nm.

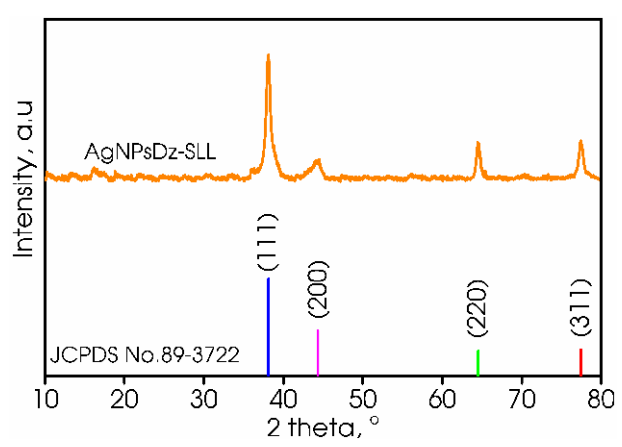


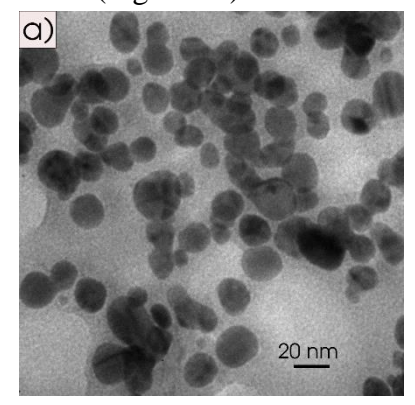
Figure 4. XRD pattern of AgNPsDz-SLL.

Table 2. The particle size from the XRD pattern of AgNPsDz-SLL.

2θ (°)	FWHM	Particle diameter, nm	Average particle diameter, nm
38.15	0.689	12.2	
44.14	0.741	11.6	14.6
64.54	0.515	18.2	14.0
77.53	0.621	16.4	

TEM image provided data about the morphology and size of the photosynthesized AgNPsDz-SLL (Figure 5). As observed in Figure 5a, the obtained nanoparticles possessed

spherical shapes and good dispersion. The mean size of AgNPsDz-SLL, whose average size was 17.4 nm (Figure 5b).



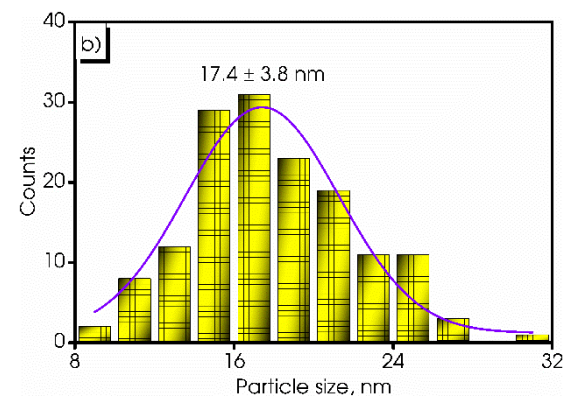


Figure 5. TEM image (a) and the distribution size (b) of AgNPsDz-SLL.

The existence of functional groups in ExtDz and AgNPsDz-SLL was revealed by FTIR spectroscopy in Figure 6a. Four major vibration bands could be observed, including the broadband at 3421 cm⁻¹ from OH deformation vibrations of the alcohols and phenolic compounds, 1633 cm⁻¹ from OH bending, 1387 cm⁻¹ from C-H symmetric deformation, and 1061 cm⁻¹ from the C-O-C- vibration band of the ether group. The presence of these functional groups indicated that the *D. zibethinus* peel extract included a variety of phytoconstituents, particularly pectin, phenolic compounds, and carbohydrates. These were considered vital reagents for reducing and stabilizing the extract-assisted synthesis [42, 43]. Furthermore, there was a distinctive decline in the transmittance of AgNPsDz-SLL compared to ExtDz, confirming that phytochemicals in the extract participated in the synthesis process and stabilized the surface of the formed spherical nanoparticles.

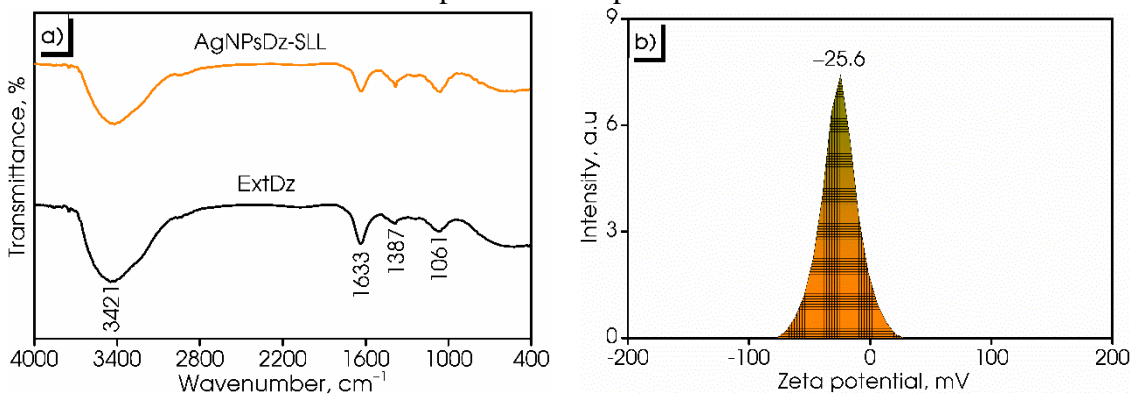


Figure 6. (a) FTIR of ExtDz and AgNPsDz-SLL; (b) the zeta potential of AgNPsDz-SLL.

The stability of the synthesized colloidal AgNPs was shown in Figure 6b by the zeta potential measurements. AgNPsDz-SLL manifested a negative value of -25.6 mV. Several phytochemicals, including flavonoids, pectin, and carbohydrates, were present in the extract as capping agents to prevent AgNP agglomeration, as evidenced by the extract's high negative zeta potential values. The zeta potential value was higher than 20 mV, which suggested that the produced AgNPs were highly stable [44].

Figure 7 and Table 3 demonstrate the inhibitory efficiency of AgNPsDz-SLL for bacteria and cancer cells. The biological activity of the produced AgNPsDz-SLL against bacteria and cancer cells was presented by the half-maximal inhibitory concentration (IC₅₀). As can be observed, microbial growth was inhibited to varying degrees based on introducing AgNP concentrations. Regarding the antibacterial properties, AgNPsDz-SLL displayed the

best inhibition activity on *L. fermentum* (IC₅₀ = 0.74 mg/L) for gram-negative bacteria and *P. aeruginosa* (IC₅₀ = 0.18 mg/L) for gram-positive bacteria; the weakest antibacterial activity was against *B. subtilis*, 64.00 mg/L AgNPs inhibited 45% *B. subtilis* growth. Order of antibacterial activity of AgNPsDz-SLL followed: *P. aeruginosa* (IC₅₀ = 0.18 mg/L) > *L. fermentum* (IC₅₀ = 0.74 mg/L) > *S. enterica* (IC₅₀ = 0.96 mg/L) < *S. aureus* (IC₅₀ = 1.82 mg/L) < *E. coli* (IC₅₀ = 9.41 mg/L) > *B. subtilis*. Involving anticancer activity, the produced AgNPsDz-SLL were effective at hindering the growth of cancer cells, including A549, HepG2, KB, and MCF7, with IC₅₀ values of 10.42-41.28 mg/L. The breast cancer cell MCF7 exhibited the greatest control of cancer cells with IC₅₀ = 10.42 mg/L.

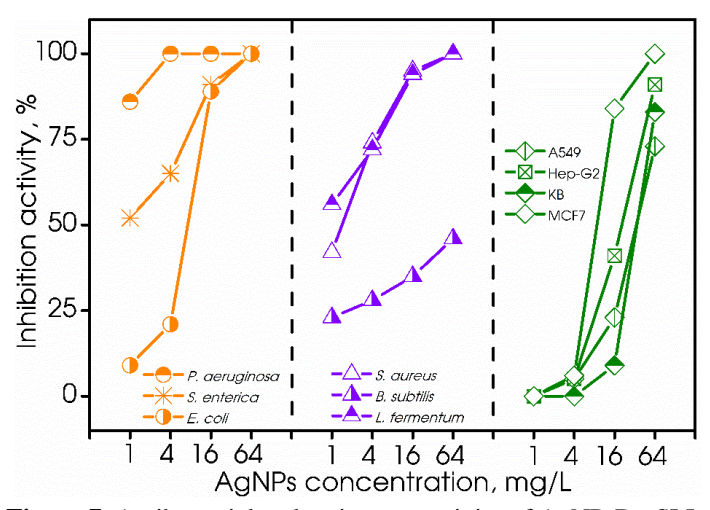


Figure 7. Antibacterial and anticancer activity of AgNPsDz-SLL.

Bacteria/cancer cells		AgNPsDz-SLL, mg/L	Control, mg/L		
			Ampicillin	Cefotaxime	Ellipticine
Common magazina	S. enterica	0.96 ± 0.04		1.42 ± 0.17	
Gram-negative bacteria	E. coli	9.41 ± 0.05		0.12 ± 0.01	
Dacterra	P. aeruginosa	0.18 ± 0.02		14.32 ± 0.50	
C	S. aureus	1.82 ± 0.07	0.07 ± 0.02		
Gram-positive bacteria	B. subtilis	-	9.95 ± 1.79		
Dacterra	L. fermentum	0.74 ± 0.04	3.40 ± 0.23		
	A549	40.62 ± 3.76			1.06 ± 0.07
Cancer cells	HepG2	23.87 ± 1.78			1.39 ± 0.13
Cancer cens	KB	41.28 ± 3.43			1.09 ± 0.07
	MCF7	10.42 ± 0.12			1.32 ± 0.10

Table 3. IC₅₀ of AgNPsDz-SLL against bacteria/cancer cells.

The sensitivity of the colorimetric assay was verified by varying various Cu²⁺ concentrations and fixing AgNP concentrations for the plant-derived AgNPsDz-SLL (Figure 8). The UV-vis absorption spectra were verified on solutions containing AgNPs with increasing Cu²⁺ concentrations (Figure 8a). The calibration curve was established by the absorbance difference of AgNPs at 422 nm (Figure 8b). The results indicated that with an increase in Cu²⁺ concentration, the absorbance value exhibited a decreasing trend, and the absorbance difference exhibited an increasing tendency. The absorbance difference has a good nonlinear relationship with Cu²⁺ concentration from 5 to 1200 µg/L for AgNPs with a correlation coefficient of 0.9921, and the LOD of Cu²⁺ was estimated to be approximately 1.8 µg/L. As can be seen, the colorimetric assay using AgNPsDz-SLL was appropriate for the recognition of low-concentration Cu²⁺. Copper is necessary in trace amounts for human health. However, abnormal levels can lead to significant toxicity, including DNA damage, peroxidation, and lipid damage. This can result in the development of various neurodegenerative diseases.

Additionally, excessive Cu^{2+} led to harmful effects and contributed to severe environmental pollution [45, 46]. According to the United States Environmental Protection Agency, a maximum contaminant level of 20 μ M Cu^{2+} in drinking water has been established [47]. Therefore, the synthesized AgNPsDz-SLL has the potential for detecting Cu^{2+} in water.

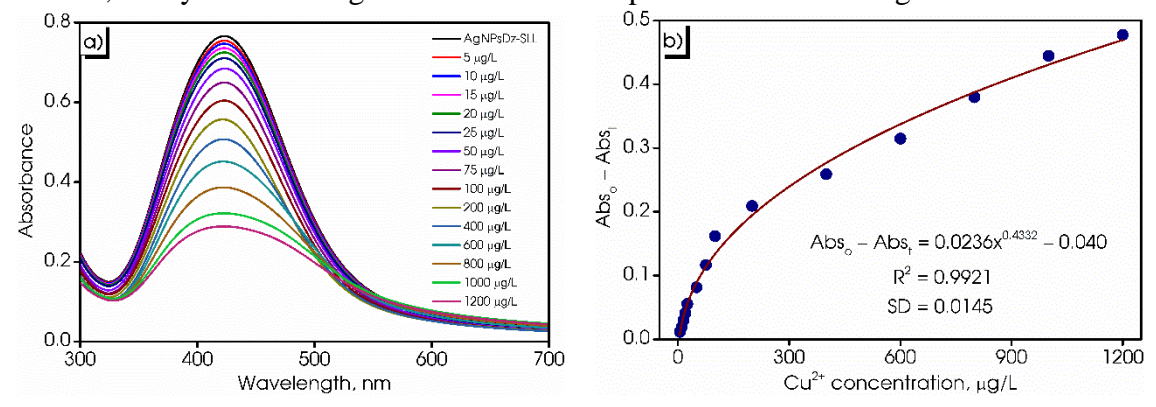


Figure 8. (a) The UV-vis absorption spectra of AgNPs with different concentrations of Cu²⁺; (b) the relationship between Cu²⁺ concentration and the absorbance difference.

Compared with recent studies for the Cu^{2+} determination in water, fluorescence and colorimetric methods exhibited better detection limits than the Raman technique (Table 4). The synthesized AgNPsDz-SLL in the present work showed a good detection limit similar to AuNPs, with LOD at 1.8 μ g/L. Also, the colorimetric method is simple, non-toxic, low-cost, has a simple operation, and rapid detection. Therefore, AgNPsDz-SLL material was a potential candidate for colorimetric detection of Cu^{2+} .

Table 1011 comparison of this work with other previously partitions stated states.						
Method	Material	Analytical ranges, μg/L	Limit of detection, µg/L	Reference		
Raman	AgNPs	64.0-64.0×10 ³	64.0	[48]		
Raman	Fe ₃ O ₄ @SiO ₂ -AgNPs	$0.5 \times 10^3 - 20.0 \times 10^3$	421.0	[49]		
Fluorescence	Carbon dots	$0-10.9\times10^{3}$	3.3	[50]		
Fluorescence	Carbon dots/AgNPs	$0-3.8\times10^3$	8.3	[51]		
Colorimetric	AuNPs	3.2-256.0	2.2	[52]		
Colorimetric	AgNPs	$0-256.0\times10^3$	42.2×10 ³	[53]		
Colorimetric	AuNPs-AgNPs	$0-10.0\times10^3$	30.0	[54]		
Colorimetric	AgNPsDz-SLL	$5.0-1.2\times10^3$	1.8	This work		

Table 4. A comparison of this work with other previously published studies.

4. Conclusions

The current study successfully utilized an aqueous peel extract from a *D. zibethinus* peel under LED artificial sunlight to synthesize AgNPs and address the agricultural waste problem. Numerous phytoconstituents in the extract are managed as potent reducing and stabilizing agents to produce small, uniformly distributed, highly durable AgNPs via a green route. The effect of photo-irradiation on AgNP synthesis was examined through certain parameters, such as the concentration of *D. zibethinus* peel extract, the extraction temperature, and the extraction duration. These influencing factors suggested the optimum condition for AgNP synthesis by 7.0 g/L of *D. zibethinus* peel powder extracted at 40°C for 20 min. AgNPsDz-SLL had a reaction efficiency of 83.4%. Additionally, the obtained AgNPsDz-SLL, whose average size was around 17.4 nm, possessed exceptional biomedical applications, such as antibacterial and anticancer activities. Also, an efficient colorimetric method was developed for the rapid Cu²⁺ detection at a low concentration (1.8 µg/L). Due to the abundance of material

and the uncomplicated process, this reliable, cost-effective, and environmentally friendly method is ideal for large-scale manufacturing and a variety of applications.

Author Contributions

Conceptualization, T.D.N., A.N.P., and N.T.-T.T.; methodology, T.D.N., A.N.P., and H.T.N.; software, G.T.-N.T., A.N.P., and T.D.N.; validation, N.T.-T.T.; formal analysis, G.T.-N.T., A.N.P., T.D.N., and N.T.-T.T.; investigation, G.T.-N.T., A.N.P., T.D.N., and H.T.N.; data curation, G.T.-N.T., A.N.P., T.D.N., and H.T.N.; writing—original draft preparation, T.D.N. and A.N.P.; writing—review and editing, G.T.-N.T., A.N.P., T.D.N., and N.T.-T.T.; supervision, T.D.N. All authors have read and agreed to the published version of the manuscript.

Institutional Review Board Statement

Not applicable.

Informed Consent Statement

Not applicable.

Data Availability Statement

Not applicable.

Funding

This study is funded in part by the Can Tho University, Code: TSV2023-24.

Acknowledgments

This work was supported by the Can Tho University.

Conflicts of Interest

The authors declare no conflict of interest.

References

- 1. Heiligtag, F.J.; Niederberger, M. The fascinating world of nanoparticle research. *Mater. Today.* **2013**, *16*, 262-271, https://doi.org/10.1016/j.mattod.2013.07.004.
- 2. Caldonazo, A.; Almeida, S.L.; Bonetti, A.F.; Lazo, R.E.L.; Mengarda, M.; Murakami, F.S. Pharmaceutical applications of starch nanoparticles: A scoping review. *Int. J. Biol. Macromol.* **2021**, *181*, 697-704, https://doi.org/10.1016/j.ijbiomac.2021.03.061.
- 3. Saravanan, A.; Kumar, P.S.; Karishma, S.; Vo, D.V.N.; Jeevanantham, S.; Yaashikaa, P.; George, C.S. A review on biosynthesis of metal nanoparticles and its environmental applications. *Chemosphere* **2021**, *264*, 128580, https://doi.org/10.1016/j.chemosphere.2020.128580.
- 4. Jamkhande, P.G.; Ghule, N.W.; Bamer, A.H.; Kalaskar, M.G. Metal nanoparticles synthesis: An overview on methods of preparation, advantages and disadvantages, and applications. *J. Drug Deliv. Sci. Technol.* **2019**, *53*, 101174, https://doi.org/10.1016/j.jddst.2019.101174.
- 5. Saif, S.; Tahir, A.; Chen, Y. Green synthesis of iron nanoparticles and their environmental applications and implications. *Nanomaterials* **2016**, *6*, 209, https://doi.org/10.3390/nano6110209.
- 6. Xiong, K.R.; Liang, Y.R.; Yi, O.Y.; Wu, D.C.; Fu, R.W. Nanohybrids of silver nanoparticles grown in-situ

- on a graphene oxide silver ion salt: Simple synthesis and their enhanced antibacterial activity. *New Carbon Mater.* **2019**, *34*, 426-433, https://doi.org/10.1016/S1872-5805(19)60024-7.
- 7. Behra, R.; Sigg, L.; Clift, M.J.; Herzog, F.; Minghetti, M.; Johnston, B.; Petri-Fink, A.; Rothen-Rutishauser, B. Bioavailability of silver nanoparticles and ions: from a chemical and biochemical perspective. *J. R. Soc. Interface* **2013**, *10*, 20130396, https://doi.org/10.1098/rsif.2013.0396.
- 8. Zhang, X.F.; Liu, Z.G.; Shen, W.; Gurunathan, S. Silver nanoparticles: synthesis, characterization, properties, applications, and therapeutic approaches. *Int. J. Mol. Sci.* **2016**, *17*, 1534, https://doi.org/10.3390/ijms17091534.
- 9. Venugopal, K.; Rather, H.; Rajagopal, K.; Shanthi, M.; Sheriff, K.; Illiyas, M.; Rather, R.; Manikandan, E.; Uvarajan, S.; Bhaskar, M. Synthesis of silver nanoparticles (AgNPs) for anticancer activities (MCF7 breast and A549 lung cell lines) of the crude extract of Syzygium aromaticum. *J. Photochem. Photobiol. B Biol.* **2017**, *167*, 282-289, https://doi.org/10.1016/j.jphotobiol.2016.12.013.
- 10. Bhattarai, B.; Zaker, Y.; Atnagulov, A.; Yoon, B.; Landman, U.; Bigioni, T.P. Chemistry and structure of silver molecular nanoparticles. *Acc. Chem. Res.* **2018**, *51*, 3104-3113, https://doi.org/10.1021/acs.accounts.8b00445.
- 11. Iravani, S.; Korbekandi, H.; Mirmohammadi, S.V.; Zolfaghari, B. Synthesis of silver nanoparticles: chemical, physical and biological methods. *Res. Pharm. Sci.* **2014**, *9*, 385-406.
- 12. 1. Dang-Bao, T.; Favier, I.; Gómez, M. Metal Nanoparticles in Polyols: Bottom-up and Top-down Syntheses and Catalytic Applications. In Nanoparticles in Catalysis; Philippot, K., Roucoux, A., Eds.; John Wiley & Sons: 2021; pp. 99-122, https://doi.org/10.1002/9783527821761.ch5.
- 13. Saklani, V.; Suman, J.V.; Jain, K. Microbial synthesis of silver nanoparticles: A review. *J. Biotechnol. Biomater.* **2012**, *13*, 1-3, https://doi.org/10.4172/2155-952X.S13-007.
- 14. Jiang, X.; Chen, C.; Chen, W.; Yu, A. Role of citric acid in the formation of silver nanoplates through a synergistic reduction approach. *Langmuir* **2010**, *26*, 4400-4408, https://doi.org/10.1021/la903470f.
- 15. Rao, Y.; Banerjee, D.; Datta, A.; Das, S.; Guin, R.; Saha, A. Gamma irradiation route to synthesis of highly re-dispersible natural polymer capped silver nanoparticles. *Radiat. Phys. Chem.* **2010**, *79*, 1240-1246, https://doi.org/10.1016/j.radphyschem.2010.07.004.
- 16. Slepička, P.; Slepičková Kasálková, N.; Siegel, J.; Kolská, Z.; Švorčík, V. Methods of gold and silver nanoparticles preparation. *Materials* **2019**, *13*, 1, https://doi.org/10.3390/ma13010001.
- 17. Zulina, N.A.; Pavlovetc, I.M.; Baranov, M.A.; Denisyuk, I.Y. Optical, structural and nonlinear optical properties of laser ablation synthesized Ag nanoparticles and photopolymer nanocomposites based on them. *Opt. Laser Technol.* **2017**, *89*, 41-45, https://doi.org/10.1016/j.optlastec.2016.09.039.
- 18. Chugh, D.; Viswamalya, V.; Das, B. Green synthesis of silver nanoparticles with algae and the importance of capping agents in the process. *J. Genet. Eng. Biotechnol.* **2021**, *19*, 126, https://doi.org/10.1186/s43141-021-00228-w.
- 19. Zuhrotun, A.; Oktaviani, D.J.; Hasanah, A.N. Biosynthesis of gold and silver nanoparticles using phytochemical compounds. *Molecules* **2023**, *28*, 3240, https://doi.org/10.3390/molecules28073240.
- 20. Giao, N.T.; Cong, D.C.; Tuong, P.T.L.; Dan, T.H.; Trinh, L.T.K. The use and management of pesticides in Paddy rice and Durian cultivation in Phong Dien District, Can Tho city, Vietnam. *J. Sci. Technol. Res.* **2021**, 3, 1-10, https://doi.org/10.37933/nipes/3.3.2021.1.
- 21. Saoraya, J.; Inboriboon, P.C. Acute poisoning surveillance in Thailand: the current state of affairs and a vision for the future. *Int. Sch. Res. Notices* **2013**, *2013*, 812836, https://doi.org/10.1155/2013/812836.
- 22. Alzahrani, E. Colorimetric detection of ammonia using synthesized silver nanoparticles from durian fruit shell. *J. Chem.* **2020**, *2020*, 4712130, https://doi.org/10.1155/2020/4712130.
- 23. Zhan, Y.F.; Hou, X.T.; Fan, L.L.; Du, Z.C.; Ch'ng, S.E.; Ng, S.M.; Thepkaysone, K.; Hao, E.W.; Deng, J.G. Chemical constituents and pharmacological effects of durian shells in ASEAN countries: A review. *Chin. Herb. Med.* **2021**, *13*, 461-471, https://doi.org/10.1016/j.chmed.2021.10.001.
- 24. Ivanova, N.V.; Trofimova, N.N.; Es' kova, L.A.; Babkin, V.A. The study of the reaction of pectin-Ag (0) nanocomposites formation. *Int. J. Carbohydr. Chem.* **2012**, 2012, 459410, https://doi.org/10.1155/2012/459410.
- 25. Chutrakulwong, F.; Thamaphat, K.; Limsuwan, P. Photo-irradiation induced green synthesis of highly stable silver nanoparticles using durian rind biomass: Effects of light intensity, exposure time and pH on silver nanoparticles formation. *J. Phys. Commun.* **2020**, *4*, 095015, https://doi.org/10.1088/2399-6528/abb4b5.
- 26. Khamhaengpol, A.; Siri, S. Fluorescent light mediated a green synthesis of silver nanoparticles using the

- protein extract of weaver ant larvae. *J. Photochem. Photobiol. B Biol.* **2016**, *163*, 337-344, https://doi.org/10.1016/j.jphotobiol.2016.09.003.
- 27. Lee, J.H.; Lim, J.M.; Velmurugan, P.; Park, Y.J.; Park, Y.J.; Bang, K.S.; Oh, B.T. Photobiologic-mediated fabrication of silver nanoparticles with antibacterial activity. *J. Photochem. Photobiol. B Biol.* **2016**, *162*, 93-99, https://doi.org/10.1016/j.jphotobiol.2016.06.029.
- 28. Sengan, M.; Veeramuthu, D.; Veerappan, A. Photosynthesis of silver nanoparticles using Durio zibethinus aqueous extract and its application in catalytic reduction of nitroaromatics, degradation of hazardous dyes and selective colorimetric sensing of mercury ions. *Mater. Res. Bull.* **2018**, *100*, 386-393, https://doi.org/10.1016/j.materresbull.2017.12.038.
- 29. Verma, S.; Rao, B.T.; Srivastava, A.; Srivastava, D.; Kaul, R.; Singh, B. A facile synthesis of broad plasmon wavelength tunable silver nanoparticles in citrate aqueous solutions by laser ablation and light irradiation. *Colloids Surf. A Physicochem. Eng. Asp.* **2017**, *527*, 23-33, https://doi.org/10.1016/j.colsurfa.2017.05.003.
- 30. Zheng, X.; Zhao, X.; Guo, D.; Tang, B.; Xu, S.; Zhao, B.; Xu, W.; Lombardi, J.R. Photochemical formation of silver nanodecahedra: Structural selection by the excitation wavelength. *Langmuir* **2009**, *25*, 3802-3807, https://doi.org/10.1021/la803814j.
- 31. Kamiloglu, S.; Sari, G.; Ozdal, T.; Capanoglu, E. Guidelines for cell viability assays. *Food Front.* **2020**, *1*, 332-349, https://doi.org/10.1002/fft2.44.
- 32. Anwar, Z.; Ali, S.A.; Shah, M.R.; Ahmed, F.; Ahmed, A.; Ijaz, U.; Afzal, H.; Ahmed, S.; Sheraz, M.A.; Usmani, M. Photochemical preparation, characterization and formation kinetics of riboflavin conjugated silver nanoparticles. *J. Mol. Struct.* **2023**, *1289*, 135863, https://doi.org/10.1016/j.molstruc.2023.135863.
- 33. Gopu, C.; Chirumamilla, P.; Kagithoju, S.; Taduri, S. Green synthesis of silver nanoparticles using Momordica cymbalaria aqueous leaf extracts and screening of their antimicrobial activity: AgNPs studies in Momordica cymbalaria. *Proc. Natl. Acad. Sci. India B Biol. Sci.* **2022**, *92*, 771-782, https://doi.org/10.1007/s40011-022-01367-x.
- 34. Koteswara Rao, P.; Vikram Babu, B.; Rama Krishna, A.; Sushma Reddi, M.; Sathish Mohan, B.; Anjani Devi, K.; Susmitha, U.; Raghava Rao, T. Green synthesis of silver nanoparticles using Litsea glutinosa L. leaves and stem extracts and their antibacterial efficacy. *J. Water Environ. Nanotechnol.* **2022**, *7*, 363-369, https://doi.org/10.22090/JWENT.2022.04.003.
- 35. Dwivedi, A.D.; Gopal, K. Biosynthesis of silver and gold nanoparticles using Chenopodium album leaf extract. *Colloids Surf. A Physicochem. Eng. Asp.* **2010**, *369*, 27-33, https://doi.org/10.1016/j.colsurfa.2010.07.020.
- 36. Torabfam, M.; Jafarizadeh-Malmiri, H. Microwave-enhanced silver nanoparticle synthesis using chitosan biopolymer: optimization of the process conditions and evaluation of their characteristics. *Green Process. Synth.* **2018**, 7, 530-537, https://doi.org/10.1515/gps-2017-0139.
- 37. Zhong, L.; Yuan, Z.; Rong, L.; Zhang, Y.; Xiong, G.; Liu, Y.; Li, C. An optimized method for extraction and characterization of phenolic compounds in Dendranthema indicum var. aromaticum flower. *Sci. Rep.* **2019**, *9*, 7745, https://doi.org/10.1038/s41598-019-44102-9.
- 38. Vishwasrao, C.; Momin, B.; Ananthanarayan, L. Green synthesis of silver nanoparticles using sapota fruit waste and evaluation of their antimicrobial activity. *Waste Biomass Valorization* **2019**, *10*, 2353-2363, https://doi.org/10.1007/s12649-018-0230-0.
- 39. Farias, C.B.B.; Ferreira Silva, A.; Diniz Rufino, R.; Moura Luna, J.; Gomes Souza, J.E.; Sarubbo, L.A. Synthesis of silver nanoparticles using a biosurfactant produced in low-cost medium as stabilizing agent. *Electron. J. Biotechnol.* **2014**, *17*, 122-125, https://doi.org/10.1016/j.ejbt.2014.04.003.
- 40. Wei, X.; Luo, M.; Li, W.; Yang, L.; Liang, X.; Xu, L.; Kong, P.; Liu, H. Synthesis of silver nanoparticles by solar irradiation of cell-free Bacillus amyloliquefaciens extracts and AgNO₃. *Bioresour. Technol.* **2012**, *103*, 273-278, https://doi.org/10.1016/j.biortech.2011.09.118.
- 41. Gopinath, V.; Priyadarshini, S.; Loke, M.F.; Arunkumar, J.; Marsili, E.; MubarakAli, D.; Velusamy, P.; Vadivelu, J. Biogenic synthesis, characterization of antibacterial silver nanoparticles and its cell cytotoxicity. *Arab. J. Chem.* **2017**, *10*, 1107-1117, https://doi.org/10.1016/j.arabjc.2015.11.011.
- 42. Chinnappan, S.; Kandasamy, S.; Arumugam, S.; Seralathan, K.K.; Thangaswamy, S.; Muthusamy, G. Biomimetic synthesis of silver nanoparticles using flower extract of Bauhinia purpurea and its antibacterial activity against clinical pathogens. *Environ. Sci. Pollut. Res.* **2018**, *25*, 963-969, https://doi.org/10.1007/s11356-017-0841-1.
- 43. Mahiuddin, M.; Saha, P.; Ochiai, B. Green synthesis and catalytic activity of silver nanoparticles based on Piper chaba stem extracts. *Nanomaterials* **2020**, *10*, 1777, https://doi.org/10.3390/nano10091777.

- 44. Sun, Q.; Cai, X.; Li, J.; Zheng, M.; Chen, Z.; Yu, C.P. Green synthesis of silver nanoparticles using tea leaf extract and evaluation of their stability and antibacterial activity. *Colloids Surf. A Physicochem. Eng. Asp.* **2014**, *444*, 226-231, https://doi.org/10.1016/j.colsurfa.2013.12.065.
- 45. Xing, Y.; Meng, X.; Wang, L.; Zhang, J.; Wu, Z.; Gong, X.; Wang, C.; Sun, H. Effects of benzotriazole on copper accumulation and toxicity in earthworm (*Eisenia fetida*). *J. Hazard. Mater.* **2018**, *351*, 330-336, https://doi.org/10.1016/j.jhazmat.2018.03.019.
- 46. Pradhan, S.H.; Liu, J.Y.; Sayes, C.M. Evaluating manganese, zinc, and copper metal toxicity on SH-SY5Y cells in establishing an idiopathic Parkinson's disease model. *Int. J. Mol. Sci.* **2023**, *24*, 16129, https://doi.org/10.3390/ijms242216129.
- 47. Kaewnok, N.; Petdum, A.; Sirirak, J.; Charoenpanich, A.; Panchan, W.; Sahasithiwat, S.; Sooksimuang, T.; Wanichacheva, N. Novel Cu²⁺-specific "Turn-ON" fluorescent probe based on [5]helicene with very large Stokes shift and its potential application in living cells. *New J. Chem.* **2018**, *42*, 5540-5547, https://doi.org/10.1039/C7NJ05176J.
- 48. Song, Y.; Ma, Z.; Fang, H.; Zhang, Q.; Zhou, Q.; Chen, Z.; Yang, H.; Wang, F. Au sputtered paper chromatography tandem Raman platform for sensitive detection of heavy metal ions. *ACS Sens.* **2020**, *5*, 1455-1464, https://doi.org/10.1021/acssensors.0c00395.
- 49. Hsieh, M.Y.; Huang, P.J. Magnetic nanoprobes for rapid detection of copper ion in aqueous environment by surface-enhanced Raman spectroscopy. *RSC Adv.* **2022**, *12*, 921-928, https://doi.org/10.1039/D1RA07482B.
- 50. Zhang, W.; Li, N.; Chang, Q.; Chen, Z.; Hu, S. Making a cup of carbon dots for ratiometric and colorimetric fluorescent detection of Cu²⁺ ions. *Colloids Surf. A Physicochem. Eng. Asp.* **2020**, *586*, 124233, https://doi.org/10.1016/j.colsurfa.2019.124233.
- 51. Yan, L.; Li, J.; Cai, H.; Shao, Y.; Zhang, G.; Chen, L.; Wang, Y.; Zong, H.; Yin, Y. Carbon dots/Ag nanoclusters-based fluorescent probe for ratiometric and visual detection of Cu²⁺. *J. Alloys Compd.* **2023**, 945, 169227, https://doi.org/10.1016/j.jallcom.2023.169227.
- 52. Zhou, H.Y.; Peng, L.J.; Tian, T.; Zhang, W.Y.; Chen, G.Y.; Zhang, H.; Yang, F.Q. Multicolor colorimetric assay for copper ion detection based on the etching of gold nanorods. *Microchim. Acta* **2022**, *189*, 420, https://doi.org/10.1007/s00604-022-05515-y.
- 53. Almaquer, F.E.P.; Perez, J.V.D. Evaluation of the colorimetric performance of unmodified citrate-stabilized silver nanoparticles for copper (II) sensing in water. *Key Eng. Mater.* **2019**, *821*, 372-378, https://doi.org/10.4028/www.scientific.net/KEM.821.372.
- 54. Thongkam, T.; Apilux, A.; Tusai, T.; Parnklang, T.; Kladsomboon, S. Thy-AuNP-AgNP hybrid systems for colorimetric determination of copper (II) ions using UV-Vis spectroscopy and smartphone-based detection. *Nanomaterials* **2022**, *12*, 1449, https://doi.org/10.3390/nano12091449.

Publisher's Note & Disclaimer

The statements, opinions, and data presented in this publication are solely those of the individual author(s) and contributor(s) and do not necessarily reflect the views of the publisher and/or the editor(s). The publisher and/or the editor(s) disclaim any responsibility for the accuracy, completeness, or reliability of the content. Neither the publisher nor the editor(s) assume any legal liability for any errors, omissions, or consequences arising from the use of the information presented in this publication. Furthermore, the publisher and/or the editor(s) disclaim any liability for any injury, damage, or loss to persons or property that may result from the use of any ideas, methods, instructions, or products mentioned in the content. Readers are encouraged to independently verify any information before relying on it, and the publisher assumes no responsibility for any consequences arising from the use of materials contained in this publication.